MIE And Flame Velocity Of Partially Oxidised Aluminium Dust

Stephane Bernard, Philippe Gillard, Fabrice Foucher, Christine Mounaïm-Rousselle

MIE and Flame velocity of partially oxidised aluminium dust

Stéphane Bernard, Philippe Gillard, Fabrice Foucher, Christine Mounaïm-Rousselle
Institut Prisme, Université d'Orléans,
63 Boulevard de Lattre de Tassigny
18020 Bourges Cedex, France
email: Stephane.Bernard@bourges.univ-orleans.fr
phone : + 33 248 23 84 74
fax : + 33 248 23 84 71

Abstract

This work presents experimental tools for the determination of Minimum Ignition Energy (MIE) and results concerning the influence of an initial oxidation state on ignition threshold energies and flame velocity. These studies are carried out with micrometric aluminium particles which are oxidised using an anodising process. The first part of this work concerns the description of the experimental devices (Hartmann tube, for MIE measurements, and constant volume combustion chamber for flame velocity measurement with using high speed recording shadowgraphy). In the second part, a review of some results obtained for the sensitivity (MIE) of aluminium particle evolution versus particle diameter, air-fuel equivalence ratio and oxide content is presented. The effect of the oxide content is demonstrated: the MIE increases with the initial oxide content. The sensitivity of oxidised dust remains relatively high for high oxide contents (17.1wt%). The flame velocity is also modified and decreases as the oxide content increases. The most important result seems to be the role of the water content contained in the oxide shell which increases the reactivity of the oxidised aluminium dust.

Keywords : DUST EXPLOSIONS, MIE, ALUMINIUM OXIDE, FLAME VELOCITY

1 Introduction

Most industrial processes handling or producing metallic or organic powder present dust explosion hazards. The prevention of these hazards can be achieved by the characterisation of the dust parameters such as minimum ignition energy (MIE), maximum rate of pressure rise (Kst), maximum explosion pressure.

MIE is usually measured using the well-known Hartmann tube or its modified apparatus such as Mike 3 (described in EN **13821**, (2002))**.**

On the other hand, the flame velocity is an important parameter for combustion codes. Methods to measure the laminar burning velocity can be classified in two groups: the "flame propagation method" and the "stationary method". The flame propagation method generally uses open tubes or closed bombs. Opened tubes (Goroshin et al. (1996), Han et al. (2000), Proust (2006)) are filled with dust clouds generated for the most part by fluidized beds at the bottom of the tube or sometimes by a vibrating sieve placed at the top of the tube. In all cases, cloud generation conditions are chosen in order to reach a low level of residual turbulence. Ignition is most often obtained by means of an electric spark, hot wire or sometimes by a small gas burner.

In a spherical bomb, the laminar burning velocity can be evaluated by the pressure time evolution during the combustion propagation and is initially applied to gases by Lewis and Von Elbe (1987). In this experiment, dust is injected by blasting (due to its high settling velocity), strongly increasing the turbulence of the cloud. The consequence is that the measured velocity is turbulent. Some authors, Bradley et al. (1988) and Silvesterini et al. (2008) have managed to obtain laminar burning velocity by optimizing injection parameters in order to reduce turbulence and finally by extrapolating the laminar burning velocity to "zero turbulence".

It appears that dust air mixtures are often assimilated to gaseous mixtures by considering that the particles are able to produce enough volatile matter in the preheated zone of the flame, in order to

be mixed with the air surrounding the particle to burn in the flame reaction zone. These concepts are well summarized by Silvestrini et al. (2008).

Concerning stationary methods, the flame is stabilized on a nozzle burner or Bunsen burner. These methods also present some drawbacks: for example, the conditions are very dependent on the burner's characteristics and the experimental set-up must be optimized in order to keep the flame locked at the top of the burner, as reported by Dahoe et al. (2002), Horton et al. (1977) or Kolbe (2001).

This work presents in the first part the experimental devices built in order to measure the MIE of dust and the flame velocity of dust explosions. In the second part, some preliminary results on this measurement applied to partially oxidised aluminium dust are given and discussed.

2 Experimental devices for MIE determination

The MIE is determined using a statistical test of Langlie (1962) and Bernard et al. (2010) performed in a Hartmann tube (see Figure 1). This tube (1.3L) and its spark generator are described in Baudry et al. (2007). Dust is deposited at the bottom of the tube and a blast of air scatters particles in the tube. After about 100 ms, the spark is triggered at 110 mm from the bottom of the tube. The air tank pressure, the delay between the air blast and the spark and the spark's duration can be modified with our spark generator controller and optimized by Baudry (2007).

The power supply was designed to produce a spark at nearly constant power (voltage and current intensity are constant). Energy, in such a case, is only proportional to the spark duration. This time could be changed over the range of 1 µs to 1 s. The break-down of the air is obtained by a

pulse of high voltage immediately relayed by low voltage. The spark energy value achieved with such an arrangement is in the range from 10 mJ to 500 J, making it possible to measure the ignition energy of the less ignitable dusts.

Figure 1

For the measurement of the MIE, cloud generation is one key to the problem. Homogeneity of the dust dispersion, dust concentration and turbulence of the cloud are the principal parameters which control the dust cloud features and thus the MIE value. This was achieved by controlling the opening time of the valve which could be adjusted between 60 ms to 1 s and optimized to obtain uniform dispersion inside the tube. The lower overpressure in the air tank (0.5 bar) and the delay between the blast and the spark generation minimized the turbulence. The delay time between blast and spark generation could be also adjusted in the range of 0 to 1000 ms. In this study, in agreement with Eckhoff 0, this delay was adjusted to 100 ms.

3 Flame velocity and measurement

3.1. Isobaric measurement

A cylindrical constant volume combustion chamber of 24.32 litters is used. Dust was injected at the bottom of the vessel with a system derived from the Hartmann tube. The explosion was observed by a high speed camera (Photron FastCam APXPCI R2) through two BK7 windows The ignition of the generated dust cloud was achieved by the spark generator controller which controls both the injection duration and the delay between injection and ignition. The spark was ignited between two elongated tungsten electrodes. Power and duration of the spark could be adjusted with the spark controller in a range of a few mJ to 500 J.

Figure 2

Injections and configuration parameters were optimized by using shadowgraphy techniques in order to observe the cloud generation by Foucher et al. (2003) and Halter et al. (2009). It was possible to visualize the dispersion of the particle and their motion. A scattering system with a stretched drop shape was tried, Figure 3a and 3b illustrate the influence of this system. In Figure 3b, agglomerates of powder had totally disappeared and the cloud seemed to be nearly homogenous.

Figure 3

3.2. Electrical ignition system

This spark generator device was used both for the Hartmann tube and the constant volume combustion chambers; its design was detailed by Bernard et al. (2010). In this paper we only recall the electrical scheme (Figure 4) and the time evolution of the voltage and current intensity of the electrical spark (Figure 5). After the arc breakdown, voltage and current intensity were constant, in these conditions and for an arc duration of more than 20 µs the energy was linear with the arc duration.

Figure 4

Figure 5

During tests in cylindrical chamber, parameters of the spark were constant and summarised in Table 1. These parameters, and especially spark energy, were chosen to guarantee the explosion of the dust every time.

Table1

3.3. Image processing

In order to determine the apparent flame velocity of the explosion, Matlab post processing was applied to the frames obtained by the high speed camera during the explosion. The intensity of each pixel was converted into a binary code in order to determine the area of the flame. Figure 6 showed the shape of the flame area. At the beginning of the explosion the flame was nearly spherical (after 10 ms), progressively the shape of the flame was deformed, probably due to convection which increases turbulence and the fact that at a microscopic scale the cloud was not homogenous (macro scale hypothesis) but discrete. The combustion propagates step by step between particles and zones with a rich mixture are probably burnt before the lean zones due to the greater distance between particles. Therefore, propagation was not spherical and it was very difficult to determine a flame radius, stretch rate or other parameters without making strong assumptions about the flame shape.

Firstly, no hypothesis on the flame shape was made and only an equivalent flame radius was estimated by considering the flame area as a disk.

Figure 6

4 Aluminium tested dusts

Aluminium powder was provided by the company, “Métaux et Chimie”, and referenced F3915. For this study, this powder was modified by a converting treatment (anodising) in order to generate an oxide coating around the aluminium particles. This method was described by Baudry 0 al. (2007). It allows producing partially oxidised aluminium dust, in batches, in the range 0.5 - 20 wt% of oxide. These content were measured by thermogravimetry analysis (TGA). The amount of oxide and residual water are given in

Table 2. The dust was previously dried for 4 hours at 200°C. The TGA measurements show that a little content of water remains trapped in the particle and this value increases with the oxide content while this value was near zero for the F3915 where the oxide content is 0.5 wt% and only

due to natural oxidation. All oxide content values were determined with accuracy of more than 0.02 wt%, and for a water content of no more than 0.005wt%.
Nine different powders were tested and their characteristics are summarized in Table 2.

Table 2

5 Results on MIE measurement

An important parameter for MIE value was the initial mass of aluminium powder lying at the bottom of the Hartman tube. When the overpressure of discharged air was introduced through the nozzle in the lower part of tube, the powder was blown through the volume of the whole vessel.

Knowing the content of oxygen in the relative volume, it was possible to evaluate the equivalence ratio of the dust cloud. This ratio (see eq.1) is a macroscopic parameter and does not describe the reality of the dispersion which in all cases produced gradients of equivalent ratio in the volume.

$$\Phi = \frac{\left(\frac{m_{Al}}{m_{O_2}}\right)}{Z_{st}}$$ Eq. 1, with $Z_{st} = \frac{4M_{Al}}{3M_{O_2}}$, M_{Al} the molar mass of aluminium and M_{O_2} the molar mass of oxygen, m_{Al} the mass of aluminium powder injected and m_{O_2} the mass of oxygen.

When the mass of Al powder increases from 190 mg to 350 mg, the equivalence ratio grows from 0.7 to 1.6. There is a strong decrease in the MIE energy in the first part of the curve (figure 7), after 1.1 the measurement is slightly intensified. The common shape of MIE for hydrocarbon/air gaseous mixtures is typically a U-curve (see figure 8). In the case of dust/air clouds, the right part of the U-curve was generally difficult to obtain because the energy of the flow needed to produce a good suspension is also enhanced. In such cases, a significant content of the initial powder still remains in the lower part of the test device and the real equivalence ratio of the dust cloud is not

the expected one. Nevertheless, when the droplet size distribution of the powder is very narrow, which was the case of the powder d (powder A was sieved between 30 and 50µm), it is possible to observe the U-shape as shown in figure 8. These differences in the MIE values are principally due to the better fluidisation of narrow size distribution powder during the cloud generation.

Figure 8

A lot of studies were focused on aluminium combustion. All of them show the importance of the oxide layer on the particle surface. To ignite the particle, the oxide layer must be cracked by the thermo-mechanical stresses allowing to the oxygen of the air to react with the aluminium vapour by Ermakov et al.(1982), and Brandford (1986). In this way, the thickness of the oxide layer and consequently the oxide content plays an important role in the ignition phenomenon of the particle. But only a few studies deal with the influence of oxide content on dust sensitivity or flame velocity. One reason is probably the difficulty of producing powder with an aluminium coating in a large range of oxide content to perform studies. In this work, this problem was solved by a sulphuric anodising of the powder by using an electrolytic process, but another problem subsists: oxidised powder is produced in batches so it is difficult to produce more than 30 g of oxidised powder. This content is enough to perform MIE measurement but only allows a few experiments in the combustion chamber. It allows the production of partially oxidised powder with an oxide content of between 1 to 17.2 wt%. The oxide is located on the surface of particles and sometimes some particles stick together. They are dried (200°C for 4 h) and sieved, the part below 50 µm is kept and tested in a Hartmann tube.

Figure 9

The MIE of oxidised aluminium powder was measured for various oxide contents. For each of them the aluminium equivalence ratio was maintained constant and equal to 1. During the test

with large oxide content, particles were charged by an electrostatic process and attracted toward the walls of the tube. The use of antistatic adhesive along the tube walls drastically reduces the phenomenon. Langlie tests were also performed for very high oxide content such as 17.2 wt%. Figure 9 presents the influence of the oxide content on the MIE which increases with the oxide content. For low oxide content, the MIE is quite the same as “non-oxidised” (only natural oxidation) aluminium particles (about 25 to 30 mJ) and is classified as very sensitive to electrostatic ignition. It is interesting to note that the MIE of highly oxidised particles such as 17.1wt% of oxide content is equal to 657 mJ: these particles are classified as sensitive to electrostatic ignition. It was also observed that some powder samples with lower oxide content have higher MIE (1460 mJ for 7.1wt% of oxide content); in this case these powders are classified insensitive to electrostatic ignition. Investigations with ATG show differences on the residual water content trapped in the oxide shell of the particle. It seems that this small content of water increases dust sensitivity. This aspect is significant on powder which contains 17,1wt% of oxide and 4.57wt% of water.

6 Flame measurement results

Figure 10 shows a typical radius time evolution during the explosion obtained with Matlab post processing. It is possible to discern three parts to this curve. The first one concerns the ignition: the spark produces a short flash which is recorded by the camera. Secondly the combustion continues but propagates very slowly. This corresponds to the example presented in Figure 6a). Progressively the flame accelerates: Sun et al. (2006) also noted this acceleration in their apparatus with a similar order of magnitude. Finally after this acceleration, a quasi linear evolution of the radius with time is obtained: the flame velocity is nearly constant. It is in this last part of the curve that the flame velocity can be measured.

Figure 10

The load of aluminium dust injected in the chamber was varied in order to modify the equivalence ratio. Figure 11 illustrates the dependence of the flame velocity with equivalence ratio. A maximum is observed for a load of 4g. This content of powder gives an equivalence ratio of about 0.65 calculated by using the assumption of uniform dust concentration in the chamber. In fact, the dispersion volume is lower, because we note that, after the cloud generation and when all particles have settled on the circular bottom of the bomb, there are hardly any particles near the walls, while dust deposit is greater near the centre of the bottom. The largest part of the uncovered zone is about 2 cm along the walls of the bomb. Therefore, the effective dispersion volume is lower and represents about 75% of the total volume with a particle concentration higher on the axes than on the edges of the dispersion volume. The maximum of the apparent flame propagation velocity observed is about 0.32 m/s. This value is not the laminar burning velocity: the expansion factor of aluminium combustion must be taken into account. Taking it into account, the value of the velocity obtained (0.015m/s <Su<0.025m/s with an expansion factor of 12) is lower than values (0.39 to 0.49 m/s) found in literature as example Silvestrini et al. (2008). To better estimate the laminar burning velocity, the stretch, turbulence etc. need to be taken into account.

Figure 11

Figure 12 presents the apparent flame velocity with the oxide content of the aluminium dust. The equivalence ratio was fixed at 0.5 for each testing case. The velocity of flame decreases with the increase of the oxide content. It seems to be linear: the flame velocity decrease is of about 40% when the oxide content is equal to 10wt%.

Figure 12

The great dispersion in measures obtain for Powder A is mainly due, for the greatest and the lowest values, to the absence of the powder scattering device during the cloud generation for these two points. All other points are obtained with the powder scattering device (see Figure 2b).

It is interesting to note that specially oxidised aluminium dust (17.2wt%-powder J) could present a flame velocity value near that of particles with low oxide content (0.5wt%- powder A). As for MIE results, one explanation is the role of the residual water contained in the dust samples (TGA measurement). In different samples, different groups of humidity content were identified. It seems that the humidity content, probably in the alumina shell around the particle, modifies combustion phenomena inducing the increase of the flame velocity.

This last remark is very interesting, whereas the effect of a high humidity level (probably more than 10 or 15 wt%) is to completely agglomerate dust and reduce the cloud generation, but a lower content (no more than 5wt%) increases the flame velocity of oxidised aluminium particles, and probably enhance the severity explosion.

7 Conclusions

In this study, traditional apparatus (i.e. Hartmann tube) combined with a statistical method developed by ourselves allows measurement of the MIE ignition energy. This experimental method was applied both in the case of organic combustible and aluminium dusts. This work provides new data obtained in the case of aluminium powders where the initial oxide content is controlled. Classical results, such as the influence of the equivalence ratio on the MIE, were confirmed. The influence of the initial oxide content was demonstrated and it was shown that the MIE increases with this parameter. Some dusts with a high oxide content (17.1 wt%) are sensitive to electrostatic ignition and present a hazard in industrial processes.

Flame velocity measurement shows that the flame velocity is reduced with the increase of oxide content, it can also be noticed that cloud generation and particle dispersion play an important role in the reproducibility of experiments. Differences on flame velocity are observed when the residual humidity of water is contained in the oxide shell of the particle. These differences are also identified for MIE. In these two cases, it seems that for a given oxide content, when the water content increases (from 1.4 to 1.7wt% for example) the flame velocity increases (from 0.25 m/s to 0.30 m/s) and the MIE decreases. It shows that the oxide shell, without water content mitigates the explosion ability of aluminium dust, but in presence of water in the oxide, which is almost always the case, this mitigation does not occur.

References

CEN, (2002); EN 13821 Potentially explosive atmospheres – Explosion prevention and protection – Determination of minimum ignition energy of dust/air mixtures, European Committee for Standardization.

Goroshin S., Bidabadi M., Lee J. H. S., (1996), Quenching distance of laminar flame in aluminum dust clouds, Combustion and Flame, Volume 105, Issues 1-2, , Pages 147-160

Han O.S., Yashima M., Matsuda T., Matsui H., Miyake A. and Ogawa T., (2000), Behaviour of flames propagating through Lycopodium dust clouds in a vertical duct, Journal of Loss Prevention in the Process Industries 13, pp. 449–457.

Proust C., (2006), Flame propagation and combustion in some dust-air mixtures, Journal of Loss Prevention in the Process Industries, Volume 19, Issue 1, , Pages 89-100.

Lewis B., Von Elbe G., FL (1987), Combustion, flames and explosions of gases (3rd ed.), Academic Press, Orlando.

Bradley, D., Chen, Z., & Swithenbank, J. R, (1988), Burning rates in turbulent fine dust–air explosions. Proceedings of the 22nd international symposium on combustion, pp. 1767–1775.

Silvestrini M., Genova B., Leon Trujillo F.J., (2008), Correlations for flame speed and explosion overpressure of dust clouds inside industrial enclosures, Journal of Loss Prevention in the Process Industries, Volume 21, Issue 4, Pages 374-392,.

Dahoe A.E., Hanjalic K. and Scarlett B., (2002), Determination of the laminar burning velocity and the Markstein length of powder–air flames, Powder Technology 122, pp. 222–238.

Horton M.D., Goodson F.P. and Smoot L.D., (1977), Characteristics of flat, laminar coal dust flames, Combustion and Flame 28 pp. 187–195.

Kolbe, M., (2001), Laminar burning velocity measurements of stabilized aluminium dust flames. Thesis, Department of Mechanical Engineering, Concordia University, Montreal, Quebec, Canada.

Langlie, H.J., (1962), A reliability test method for one shot items. Ford Motor Company Aeronutronic Publication n°U.1792.

Bernard S., Lebecki K., Gillard P., Youinou L., Baudry G., (2010), Statistical Method for the Determination of the Ignition Energy of Dust Cloud- Experimental Validation, Journal of loss prevention in the process industries, Volume 23, Issue 3, pp 404-411.

Baudry G., Bernard S. and Gillard P. (2007), Influence of the oxide content on the ignition energies of aluminium powders, Journal of Loss Prevention in the Process Industries, Volume 20, Issues 4-6, Pages 330-336.

Baudry G. (2007), “Etude de l’explosibilité de poussières métalliques”, Thesis of the University of Orléans, France.

Eckhoff R.K., (2005); Explosion hazards in the process industries. Gulf Publishing Company. ISBN 0-9765113-4-7.

Foucher F., Burnel S., Mounaïm-Rousselle C., Boukhalfa M., Renou B., Trinité M., (2003), Flame wall interaction: effect of stretch , Experimental Thermal and Fluid Science, : vol 27/4 , pp 431 – 437.

Halter F., Foucher F., Landry L., Mounaïm-Rousselle C., (2009), Effect of dilution by Nitrogen and/or Carbon dioxide on methane and iso-octane air flame, Comb. Science Tech., Vol 181/6, pp 813-827.

Baudry G., Bernard B. Gillard P., (2007), Flammability data measurement of aluminium, powder and oxide content influence. ICDERS 21 Poitiers, France.

Ermakov V.A. AA Razdobreev, A. l. Skorik, VV Pozdeev, and SS Smoliakov., (1982), Temperature of Aluminium Particles at the Time of Ignition and Combustion. Fizika Goreinya I Vzryva, Vol. 18, N°2, pp 141-143.

Brandford J.W. (1986), Ignition and combustion temperatures determined by laser heating. Flammability and sensitivity of materials in oxygen-enriched atmospheres: ASTM STP 910, 2nd Volume, M.A. BENNING, Ed., ASTM, Philadelphia, pp 78-97.

Sun J., Dobashi R., Hirano T., (2006), Structure of flames propagating through aluminum particles cloud and combustion process of particles, Journal of Loss Prevention in the Process Industries, Volume 19, Issue 6, Pages 769-773

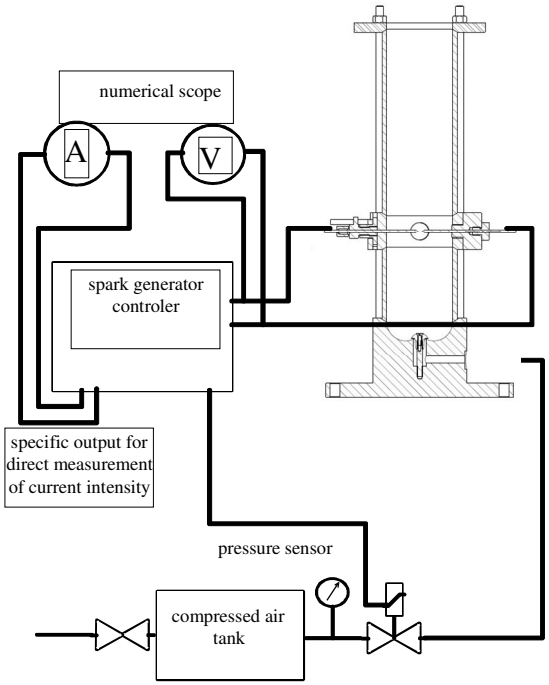

Figure 1: Hartmann tube and spark generator for MIE measurement

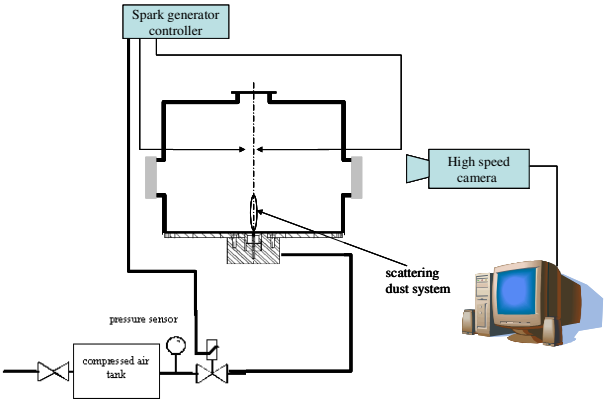

a)

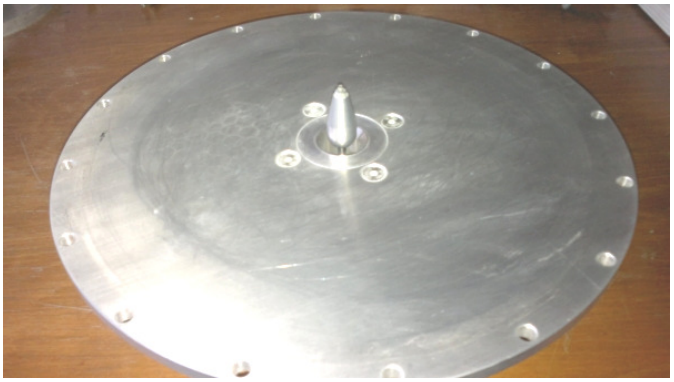

b)

Figure 2 : Cylindrical isobaric bomb device, a), System b) Photography of the scattering device

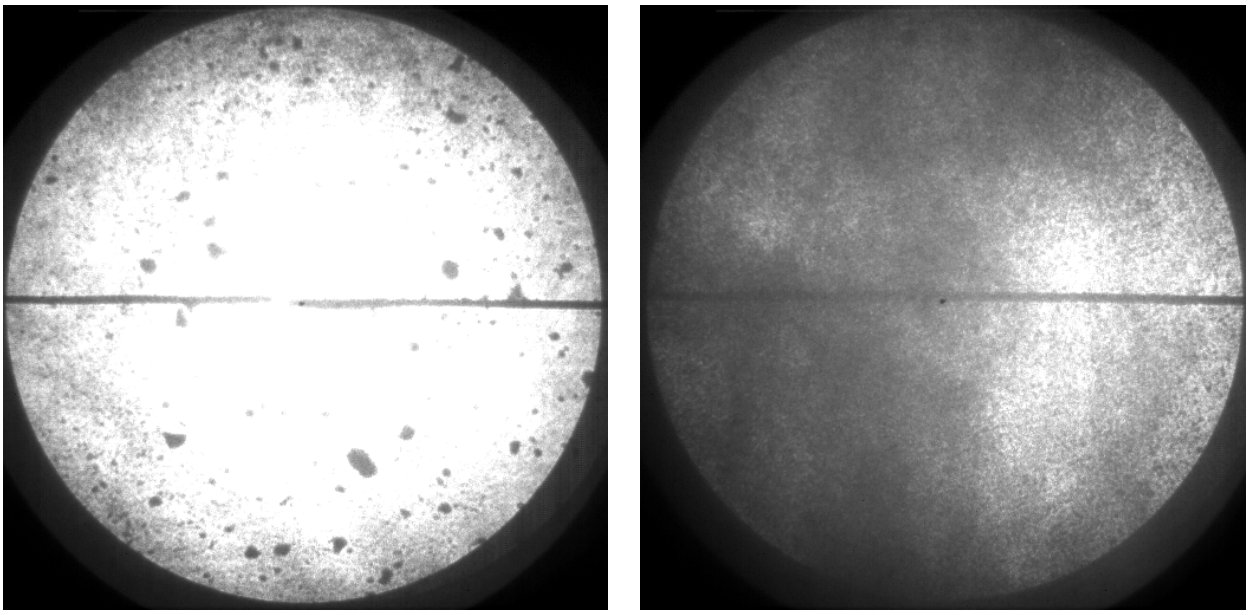

a) b)

Figure 3 : aluminium dust cloud generation observed by shadowgraphy, a) without scattering dust system, b) with scattering dust system

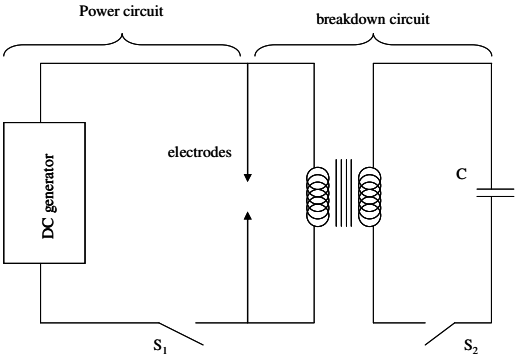

Figure 4 : electric scheme of the spark generator

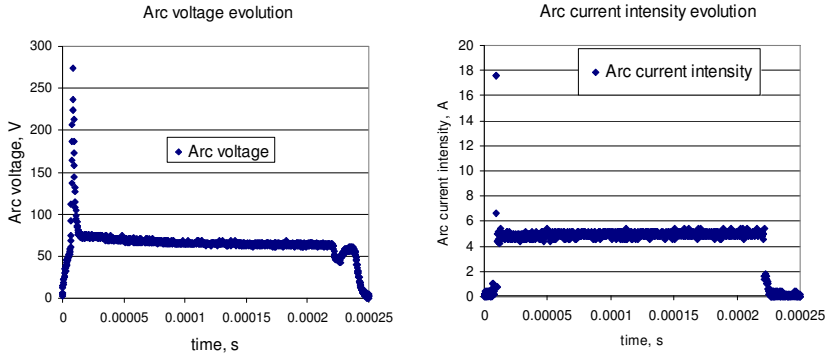

Figure 5 : Voltage and current intensity time evolution of the spark

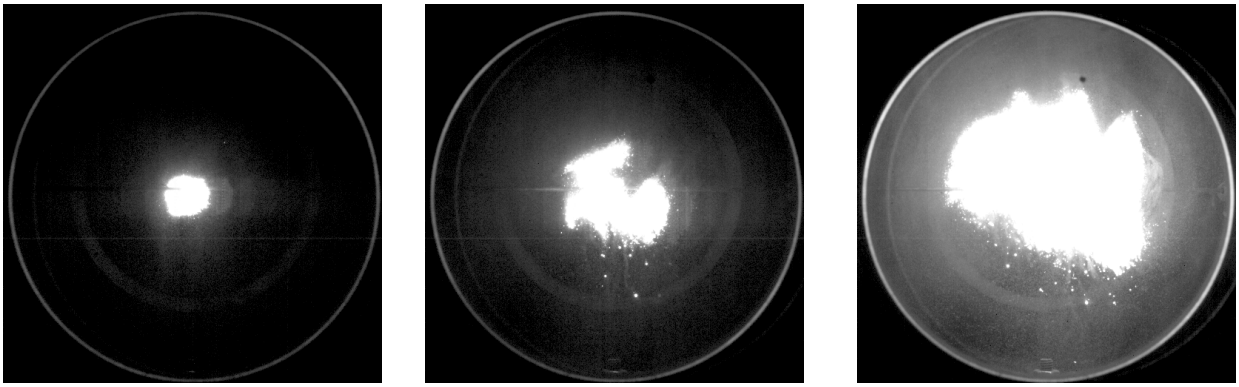

a) b) c)

Figure 6 : Example of images of an explosion of aluminium dust at different times after ignition, a) t=10ms, b) t=80ms, c) t=130ms.

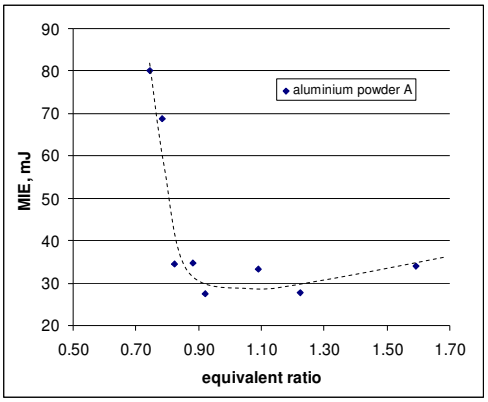

Figure 7: Minimum Ignition Energy (MIE) plotted against aluminium equivalence ratio (Powder A)

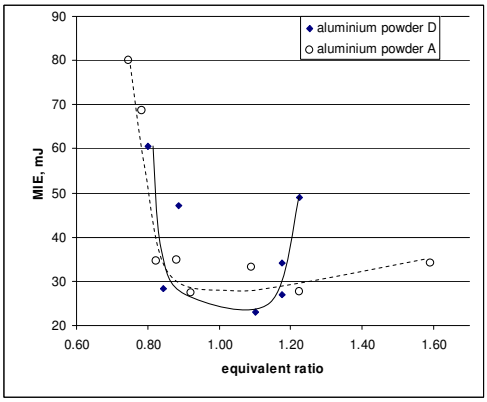

Figure 8: Minimum Ignition Energy (MIE) plotted against aluminium equivalence ratio for narrow granulometric range (Powder A sieved 30-50µm)

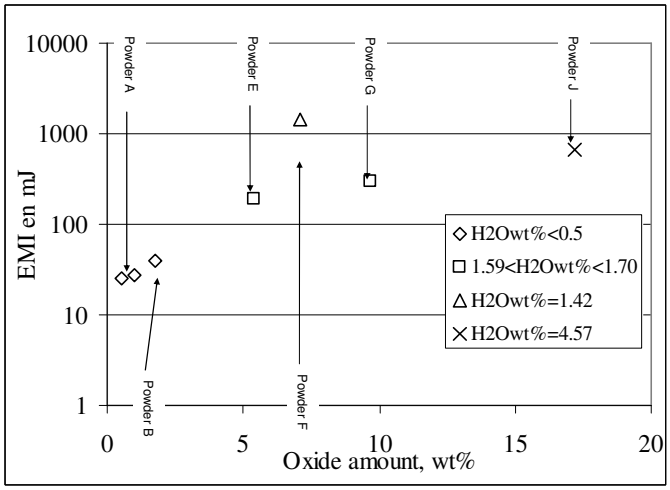

Figure 9: Influence the oxidation initial content on the MIE energy threshold

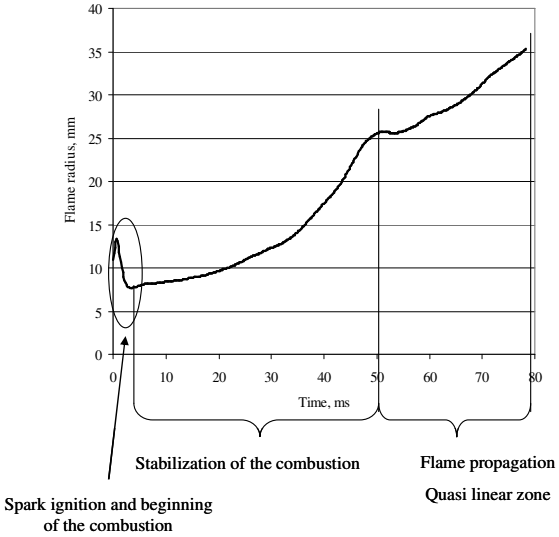

Figure 10 : Typical radius time evolution obtained with Matlab post processing applied to the combustion images.

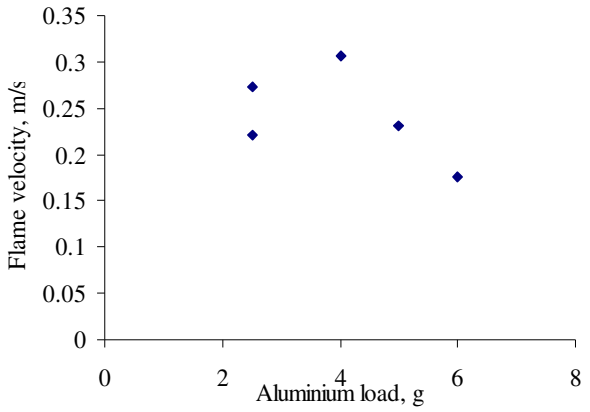

Figure 11 : Flame velocity evolution versus the aluminium load for powder A

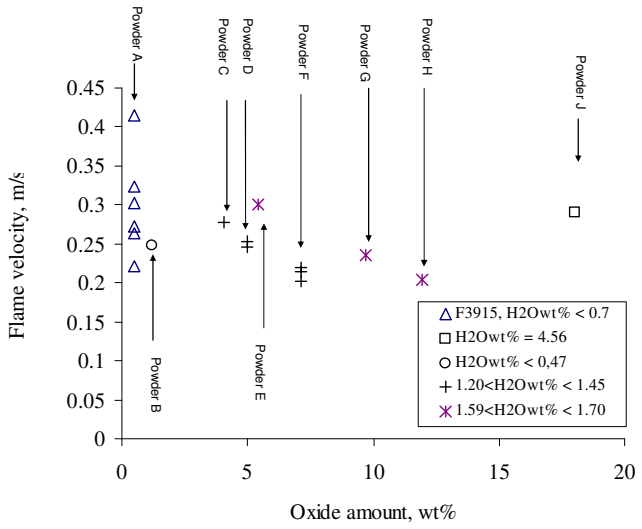

Figure 12 : Apparent flame velocity evolution with oxide content and for various water contents.

Spark current intensity, A	5,6
Spark power, W	330
Spark energy, J	50
Electrode gap, mm	4
Electrode shape	conical (40°)

Table 1: Ignition conditions

Sample	Granulometric range, µm	Oxide content, wt%	H_2O content, wt%
Aluminium powder (original) noted A	D_{v10}=7.5µm D_{v90}=60.8µm	0.5	<0.7
Oxidised Aluminium powder noted B	<50µm	1.2	0.46
Oxidised Aluminium powder noted C	<50µm	4.0	1.23
Oxidised Aluminium powder noted D	<50µm	5.0	1.42
Oxidised Aluminium powder noted E	<50µm	5.4	1.68
Oxidised Aluminium powder noted F	<50µm	7.1	1.42
Oxidised Aluminium powder noted G	<50µm	9.7	1.59
Oxidised Aluminium powder noted H	<50µm	11.9	1.70
Oxidised Aluminium powder noted J	<50µm	17.2	4.57

Table 2: Characteristics of tested dusts.